ACS Catalysis

Research Article

Cite This: ACS Catal. 2019, 9, 4875−4886

pubs.acs.org/acscatalysis

Single-Site Vanadyl Species Isolated within Molybdenum Oxide Monolayers in Propane Oxidation

Teng Fu,[†,∥] Yuanqing Wang,[†,‡] Anna Wernbacher,[†] Robert Schlögl,[†,§] and Annette Trunschke*[,†]

[†]Department of Inorganic Chemistry, Fritz-Haber-Institut der Max-Planck-Gesellschaft, Faradayweg 4-6, 14195 Berlin, Germany

[‡]BasCat - UniCat BASF JointLab, Technische Universität Berlin, Sekr. EW K 01, Hardenbergstraße 36, 10623 Berlin, Germany

[§]Department of Heterogeneous Reactions, Max-Planck-Institut für Chemische Energiekonversion, Stiftstraße 34-36, 45470 Mülheim a. d. Ruhr, Germany

Supporting Information

ABSTRACT: The cooperation of metal oxide subunits in complex mixed metal oxide catalysts for selective oxidation of alkanes still needs deeper understanding to allow for a rational tuning of catalyst performance. Herein we analyze the interaction between vanadium and molybdenum oxide species in a monolayer supported on mesoporous silica SBA-15. Catalysts with variable Mo/V ratio between 10 and 1 were studied in the oxidation of propane and characterized by FTIR, Raman, and EPR spectroscopies, temperature-programmed reduction, UV/vis spectroscopy in combination with DFT calculations, and time-resolved experiments to analyze the redox properties of the catalysts. Molybdenum oxide (sub)monolayers on silica contain mainly dioxo $(Si-O-)_2Mo(=O)_2$ species. Dilution of silica-supported vanadium oxide species by $(Si-O-)_2Mo(=O)_2$ prevents the formation of V−O−V bonds, which are abundant in the pure vanadium oxide catalyst that predominantly contains two-dimensional vanadium oxide oligomers. Existing single vanadyl $(Si-O-)_3V(=O)$ sites and neighboring $(Si-O-)_2Mo(=O)_2$ sites do not strongly interact. The rates of reduction in propane and of oxidation in oxygen are lower for single metal oxide sites compared to those for oligomers. The rate of propane oxidation correlates with the overall redox rates of the catalysts but not linearly with the chemical composition. Retarded redox behavior facilitates selectivity toward acrolein on single-site catalysts. The abundance of M−O−M bonds is more important in terms of activity and selectivity compared to the nature of the central atom (molybdenum versus vanadium).

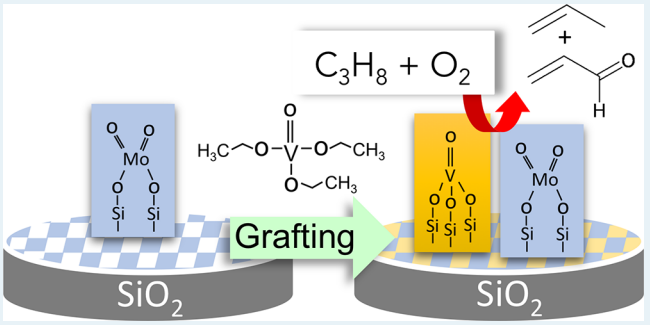

KEYWORDS: *vanadium oxide, molybdenum oxide, selective oxidation, monolayer, acrolein*

INTRODUCTION

Transition metal oxide-based catalysts containing molybdenum and vanadium have been intensively investigated in the activation of short-chain alkanes and their oxidative dehydrogenation or selective oxidation.[1−4] Generally, it has been assumed that vanadium is the element that is responsible for C−H activation and that dominates catalytic activity of V-containing mixed metal oxides.[2,4] One prominent example of a highly active and selective catalyst in ethane oxidative dehydrogenation to ethylene, propane selective oxidation to acrylic acid, and ammoxidation to acrylonitril is the Mo−V−Te−Nb oxide composed of the so-called M1 structure.[5,6] The surface of crystalline mixed Mo−V−(Te−Nb) oxide catalysts under reaction conditions of propane oxidation to acrylic acid is enriched in V^{5+}, whereas molybdenum is present in the oxidation state 6+.[7−9] The presence of surface oxide species other than vanadia may, however, affect the reaction pathways of alkanes and reaction intermediates.[10]

MoO_3 itself activates alkanes as well,[11−15] albeit at lower reaction rates.[16] Addition of promoters increases the activity of molybdenum oxide based catalysts.[17] The impact of the interaction between supported molybdenum and vanadium oxide species on reaction rates in alkane oxidation has been studied before.[15,18−23] However, in most of the investigations oxide carriers such as titania, alumina, or zirconia have been used that exhibit strong interaction with the supported phase including the formation of mixed bulk phases.[24] In contrast, the interaction of supported metal oxide species with silica is comparatively weak. Therefore, meso-structured SiO_2 (SBA-15) was selected as a carrier in the present study. The mutual interaction of supported vanadium and molybdenum oxide species in a joint monolayer was investigated. A series of near-monolayer catalysts that contain Mo and V in a variable ratio between 10 and 1 was synthesized. Catalytic performance and spectroscopic characteristics indicate the stabilization of single-site vanadyl species within the monolayer of isolated

Received: January 23, 2019
Revised: April 16, 2019
Published: April 18, 2019

DOI: 10.1021/acscatal.9b00326
ACS Catal. 2019, 9, 4875−4886

molybdenum dioxo moieties on the surface of the mixed metal oxide catalysts. Dilution with Mo prevents the formation of V−O−V bonds present in the pure silica-supported vanadia catalyst. The properties of diluted silica-supported vanadia catalysts are largely governed by the redox properties of isolated vanadium oxide species. Implications of single-site formation on activity and selectivity in propane oxidation will be discussed.

EXPERIMENTAL SECTION

Catalyst Preparation. Mesoporous silica SBA-15 was prepared according to a procedure published previously.[25] In detail, 40 g of the triblock copolymer $EO_{20}PO_{70}EO_{20}$ (EO = ethylene glycol, PO = propylene glycol, BASF Pluronic P123, Sigma-Aldrich) were added to 1350 mL 1.6 M HCl (Sigma-Aldrich) under stirring (250 rpm) at room temperature for 3 h until a homogeneous mixture was obtained. After that, 88 mL tetraethyl orthosilicate (TEOS) (Sigma-Aldrich, > 99%) were dropped into the system while the stirring at 308 K was maintained for 20 h. The gel was aged under stirring at 358 K for 24 h. The product was filtered and washed with distilled water for several times until the pH value of the washing solution reached 6.5, dried at 383 K for 16 h, and finally calcined under static air at 823 K for 12 h applying a heating rate of 1 K/min resulting in mesoporous silica SBA-15 in a batch size of 21.5 g (internal ID 22886).

Molybdenum and vanadium oxide species were supported on the single batch of mesoporous silica SBA-15 in two different consecutive steps. At first, a series of silica-supported molybdenum oxide catalysts was prepared by employing an anion-exchange procedure,[26] which requires the functionalization of the silica surface with propylammonium chloride.

For functionalization, 10 g SBA-15 and 26 g (3-aminopropyl) trimethoxysilane (ATPMS) (Sigma-Aldrich, > 97%) were suspended in 400 mL toluene (Sigma-Aldrich). The mixture was stirred at 338 K for 12 h. After that, the product was filtered and washed 5 times with 100 mL toluene and then dried at room temperature in static air for 16 h. The dried powder was then suspended in 600 mL 0.3 M HCl and stirred at room temperature for another 12 h. Finally the functionalized SBA-15 was filtered and washed 5 times with 100 mL water and dried at 353 K in static air.

For synthesis of the supported molybdenum oxide catalysts, typically 2.5 g of functionalized SBA-15 and an appropriate amount of ammonium heptamolybdate tetrahydrate (AHM) (Sigma-Aldrich, >99.9%) were suspended in 60 mL H_2O and stirred at room temperature for 12 h. The sample was filtered and washed with H_2O once and then dried at 373 K. Finally the sample was calcined at 823 K for 8 h (1 K/min) in static air. The four catalysts 4Mo, 6Mo, 8Mo, and 10Mo (internal ID 22950, 22958, 22962, 22975, respectively) were denoted as mMo; *m* represents the nominal Mo loading (wt %) calculated according to the amount of added AHM.

The silica-supported Mo−V oxide catalysts were synthesized starting from the freshly calcined silica-supported molybdenum oxide catalysts employing a grafting method by using vanadium oxytriethoxide (Sigma-Aldrich, >95%) dissolved in toluene as a vanadium precursor. The catalysts were denoted as mMo-nV, *n* represents the nominal V loading (wt %).

To estimate the required amount of vanadium precursor, the number of residual hydroxyl groups in the mMo catalysts was determined by a combination of thermal analysis and infrared spectroscopy. At first, the concentration of surface hydroxyl groups in pure SBA-15 was measured taking into account the mass loss in thermal analysis between 823 and 1473 K and assuming that one water molecule is formed by condensation of two hydroxyl groups. The concentration was used to calibrate the peak area of OH groups in the infrared spectrum of pure SBA-15 (integration range of 3680−3765 cm^{-1}). Subsequently, the concentration of residual OH groups in the mMo catalysts was estimated using this calibration factor for analysis of the peak area of the silanol peak in the infrared spectra of the mMo catalysts after calcination at 823 K applying the same integration range. The method provides only a rough estimation influenced by possible hydrogen bonding between OH groups and supported metal oxide species.

In an attempt to achieve a complete Mo−V oxide monolayer, the amount of the vanadium oxytriethoxide precursor added was estimated based on half of the molar amount of residual hydroxyl groups present on the surface of the corresponding mMo catalyst assuming that one vanadium precursor molecule in solution reacts with two surface silanol groups. In total, four supported mixed oxide catalysts were prepared by varying the nominal molar Mo:V ratio from 1 in 4Mo-4V (internal ID 23246) to 2 in 6Mo-3V (internal ID 23247), 4 in 8Mo-2V (internal ID 23274), and 10 in 10Mo-1V (internal ID 23281). A reference catalyst that contains only supported vanadium oxide species 4V (internal ID 23087) was prepared according to the same grafting procedure using the calcined SBA-15 as support. Typically, 1.5 g of the corresponding mMo catalyst or pure SBA-15, respectively, were suspended in 150 mL toluene and boiled under reflux for 5 h under Ar flow to remove residual adsorbed water. Subsequently, the suspension was cooled to room temperature and an appropriate amount of vanadium oxytriethoxide (Sigma-Aldrich, > 95%) was added followed by refluxing for another 12 h under Ar flow (20 mL/min). Subsequently, the suspension was filtered and washed 2 times with 100 mL toluene to remove the residual vanadium oxytriethoxide. The solvent was evaporated at room temperature. Finally the sample was calcined in static air at 823 K for 12 h, applying a heating rate of 1 K/min.

Catalyst Characterization and Model Calculations. Specific surface area and porosity were analyzed by nitrogen adsorption performed at 77 K using the Autosorb-6B analyzer (Quantachrome) after outgassing the catalysts in vacuum (2 h at 473 K). All data treatments were performed using the Quantachrome Autosorb software package. The specific surface area A_s (total surface area) was calculated according to the multipoint Brunauer−Emmett−Teller method (BET) in the p/p_0 = 0.05−0.15 pressure range assuming the N_2 cross sectional area of 16.2 $Å^2$. The pore size distribution was determined by the NLDFT method using a model based on equilibrated adsorption of N_2 on silica under assumption of cylindrical pores. The micropore surface area was estimated using the *t*-plot method applying a statistical thickness in the range of t = 4.5−6.5 Å.

Thermogravimetry (TG) was used to determine the concentration of silanol groups on the surface of calcined SBA-15 applying a Netzsch STA449 Jupiter thermo analyzer. At first, the support was freshly calcined in air at 823 K. Then, the sample was transferred to the balance and heated to 823 K in Argon flow with a heating rate of 10 K min^{-1}. The temperature was maintained for 1 h and subsequently raised with 10 K min^{-1} to 1473 K and held for 30 min. The

DOI: 10.1021/acscatal.9b00326
ACS Catal. 2019, 9, 4875−4886

concentration of residual surface hydroxyl groups after calcination at 823 K was calculated based on the mass loss between 823 and 1473 K assuming that one water molecule is formed by the condensation of two hydroxyl groups.

The vanadium and molybdenum content was analyzed by X-ray fluorescence (XRF) on a Bruker S4 Pioneer X-ray spectrometer. For sample preparation, the mixture of 0.05 g catalyst and 8.9 g lithium tetraborate (>99.995%, Aldrich) was fused into a disk using an automated fusion machine (Vulcan 2 MA, Fluxana).

FTIR spectra were collected at beam temperature on a Varian 670 spectrometer equipped with a liquid nitrogen-cooled MCT detector at a resolution of 4 cm^{-1} accumulating 512 scans. The catalysts were pressed into self-supported wafers (area weight approximately 10 mg/cm^2), heated under vacuum to 823 K with a heating rate of 10 K min^{-1}, and treated under these conditions for 30 min. After that, an equilibrium pressure of 200 mbar O_2 was introduced into the cell and the system was kept under this condition for 1 h. The spectra were recorded after cooling in oxygen to the beam temperature.

Absorption spectra in the UV/vis range were recorded at room temperature in diffuse reflectance using a Cary 5000 instrument (Agilent) equipped with an in situ cell (Harrick Praying MantisTM diffuse reflectance attachment DRP-P72 in combination with a HVC-VUV reaction chamber). The sample was calcined at 823 K in 20% O_2 in He flow (20 mL min^{-1}). Dehydrated SBA-15 was used as a white standard. The maximum value of the Kubelka−Munk function $F(R)$ was kept below 1 by diluting the sample with SBA-15.

Time-resolved in situ UV/vis spectra of undiluted, in situ calcined catalysts were recorded using the Cary 5000 instrument (Agilent) at 693 K and a total flow rate of 20 mL min^{-1} by switching the flow from O_2/He (20/80) to C_3H_8/He (20/80), and back to O_2/He (20/80). During the transient state the $F(R)$ value was recorded at 700 nm by using the kinetic mode of the spectrometer software in order to observe continuous change, with a time resolution of 2×10^{-3} s^{-1}.[27,28] For the calculation of the initial reduction rate, a period of 180 s was analyzed by linear fitting starting 120 s after the onset of increasing $\Delta F(R)$. For the calculation of the initial oxidation rate, a period of 25 s was analyzed by linear fitting starting 5 s after the onset of decreasing of $\Delta F(R)$.

Raman spectra were recorded applying a 532 nm laser. A confocal microscope (S&I GmbH, Warstein, Germany) equipped with a liquid nitrogen-cooled CCD detector (PyLoN:2K from Princeton Instruments) was used. The beam was focused with a 10× objective (Olympus) applying a laser power of 0.5 mW and exposure times of 1800 s. Under these optimized measurement conditions, no beam damage was observed. Before measurement at room temperature, the catalysts were calcined in a CCR1000 reactor cell (Linkam Scientific, Tadworth, UK) at 823 K in 20% O_2 in He flow (20 mL min^{-1}) to remove adsorbed water.

Temperature-programmed reduction with hydrogen (H_2-TPR) was performed with the freshly calcined catalysts using a tubular quartz reactor. After pretreatment at 823 K (heating rate 10 K min^{-1}) for 0.5 h in 20% O_2 in He flow (20 mL min^{-1}), consumption of hydrogen during heating in 5% H_2/Ar (50 mL min^{-1}, 423 to 1253 K, heating rate 5 K min^{-1}) was recorded applying a TCD detector. The sample weight was varied to keep the total amount of molybdenum and vanadium in the reactor constant at about 50 μmol. The hydrogen consumption was calculated based on the integration between 600−1200 K and using CuO as standard.

EPR spectra were recorded on a Bruker EMXplus spectrometer equipped with a Bruker ER 4119 HS resonator and a Bruker EMXPremiumX microwave bridge. Samples were measured in Sigma-Aldrich Wilmad quartz (CFQ) EPR tubes (o.d. 4 mm) at 110 K using a microwave frequency of 9.44−9.45 GHz (X-band) at a microwave power of 2 mW, a modulation frequency of 100 kHz, and a modulation amplitude of 0.5 mT. The spectra of catalysts in the hydrated state were collected without any pretreatment. Dehydrated catalysts were measured after pretreatment at 823 K in dynamic vacuum, addition of 200 mbar O_2, and subsequent evacuation at 823 K. Reduction was performed by heating at 693 K in dynamic vacuum followed by addition of 100 mbar C_3H_8 and subsequent evacuation at 693 K.

Oxidative dehydrogenation (ODH) of propane was measured at atmospheric pressure in a parallel reactor equipped with 8 fixed bed quartz reactors (6 mm inner diameter). The catalysts were pressed under ∼55 MPa, crushed and sieved to a particle size of 250−355 μm. The catalyst mass was 100 mg, and the total flow was varied between 10 and 20 mL min^{-1} resulting in W/F = 0.3−0.6 g s ml^{-1}. The temperature was measured inside the catalyst bed with a thermocouple and varied between 673 and 733 K. The feed was composed of 10% C_3H_8, 5% O_2, and 85% N_2. Products were analyzed using an online gas chromatograph (Agilent 7890A) equipped with a combination of Plot-Q (length 30 m, 0.53 mm internal diameter, 40 μm film thickness) and Plot-MoleSieve 5A columns (30 m length, 0.53 mm internal diameter, 50 μm film thickness) connected to a thermal conductivity detector (TCD) for analysis of the permanent gases CO, CO_2, N_2, O_2, and CH_4. A system of a FFAP (length 30 m, 0.53 mm internal diameter, 1 μm film thickness) and a Plot-Q column (length 30 m, 0.53 mm internal diameter, 40 μm film thickness) connected to a flame ionization detector (FID) was used to analyze C2−C3 hydrocarbons and oxygenates.

Model calculations were performed applying cluster models of supported Mo and Mo−V catalysts that have been generated in previous studies.[29−31] Calculations were performed using Gaussian 09 packages.[32] The Becke three-parameter hybrid functional with Lee−Yang−Parr correlation functional (B3LYP) together with Grimme's dispersion correction were chosen for the calculations.[33] The LANL2DZ basis set associated with the pseudopotential[34−36] was adopted for Mo and V atoms, and the 6-311+G(d,p) basis set was adopted for the other atoms. Geometries were examined by frequency calculation to show no imaginary frequency. On the basis of the geometries obtained, the corresponding absorption spectra were calculated by time-dependent density functional theory (TD-DFT).[37] In total 100 excited states were solved in TD-DFT calculations. A Lorentzian broadening of 0.2 eV was used for all the calculated spectra. Raman spectra were also generated for the obtained geometries with a scaling factor of 0.934[38] and Lorentzian broadening (fwhm: 10 cm^{-1}). All images are generated from GaussView 6.

RESULTS AND DISCUSSION

Structure of the Supported Metal Oxide Species. Decoration of the SBA-15 surface by molybdenum−vanadium oxide monolayers has an impact on the porosity of the support. Decreasing micropore surface area with increasing metal oxide

DOI: 10.1021/acscatal.9b00326
ACS Catal. 2019, 9, 4875−4886

Table 1. Composition, Density of Surface Species, and Surface Area of the Catalysts

				surface density				
catalyst	ID	Mo[a] loading (wt %)	V[a] loading (wt %)	Mo[b] (nm^{-2})	V[b] (nm^{-2})	OH[c] (nm^{-2})	total A_s (m^2/g)	micropores A_s (m^2/g)
SBA-15	22886	0	0	0	0	1.4[d]	1011	389
4Mo	22950	4.38	0	0.4	0	0.7	667	193
6Mo	22958	7.03	0	0.7	0	0.5	606	162
8Mo	22962	9.07	0	1.1	0	0.3	533	140
10Mo	22975	11.21	0	1.5	0	0.2	464	86
4Mo-4V	23246	4.08	3.36	0.5	0.8	0.4	522	105
6Mo-3V	23247	6.09	2.29	0.8	0.6	0.2	481	91
8Mo-2V	23274	8.18	1.73	1.3	0.5	0.1	406	48
10Mo-1V	23281	9.51	0.99	1.8	0.4	0	327	0
4V	23087	0	4.12	0	0.7	0.5	679	185

[a]Determined by XRF. [b]Based on metal loading (wt %) divided by the total specific surface area A_s of the corresponding catalyst. [c]Determined by FTIR spectroscopy using the band area between 3765−3500 cm^{-1} except for pure SBA-15. [d]Calculated based on the mass loss between 823 and 1473 K determined by thermal analysis assuming that one water molecule is formed by the condensation of two hydroxyl groups and total A_s of SBA-15.

surface coverage (Table 1) reveals a certain preference of the metal oxides species to occupy the micropores of SBA-15.

The actual Mo loading analyzed by XRF exceeds the nominal loading, while the V loading is generally lower than expected except for the Mo-free reference catalyst 4V (Table 1).

MoO_x/SiO_2. Ion exchange and grafting experiments were designed assuming that the silanol groups of the support react with the metal oxide precursor molecules. As the Mo loading increases, the density of residual hydroxyl groups decreases (Table 1). The number of OH groups consumed by anchoring one Mo atom varies between 2.4 for 4Mo and 1.6 for 10Mo (Figure S1, panels a and b). The error in determining these numbers is rather big and includes integration errors and changes in the extinction coefficient of the silanol band due to interaction of Si−OH groups with neighboring molybdenum oxo species.[11] The general trend, however, may suggest that at lower Mo loadings some mono-oxo $(Si-O-)_4Mo(=O)$ species are formed under involvement of silanol nests. At higher loadings, monografted $(Si-O)Mo(=O)_2OH$ species that contain Mo−OH groups anchored on nonvicinal silanol groups might contribute (Figure S1, panels a and b).[39] Previous NMR investigations, however, provided no evidence for Mo−OH groups in dehydroxylated silica-supported molybdenum oxide catalysts prepared in the same way.[40] Taking into account these results, the formation of dioxo $(Si-O-)_2Mo(=O)_2$ species as predominant surface molybdenum oxide structures with an average OH/Mo stoichiometry of 2 is assumed for all loadings.[11,29,40]

This is also in agreement with the Raman spectra (Figure 1a) that show only marginal contributions at wavenumbers >1010 cm^{-1}, where the Mo=O stretching vibration in mono-oxo $(Si-O-)_4Mo(=O)$ species with molybdenum in tetragonal pyramidal coordination[39,41−46] and the corresponding breathing vibration of the MoO_5 moiety[45] are expected, in particular not for the lower loaded catalysts where the formation of such a species is more likely. A double peak structure is observed with a maximum at 974 cm^{-1} attributed to the asymmetric O=Mo=O stretching vibration and the corresponding peak due to the symmetric O=Mo=O stretching vibration of dioxo $(Si-O-)_2Mo(=O)_2$ species in the range of 988−998 cm^{-1}. The presence of dioxo $(Si-O-)_2Mo(=O)_2$ species is also supported by the appearance of peaks at 367 and 190 cm^{-1} due to corresponding O=Mo=O bending and twisting vibrations, respectively (Figures S2a and S4, panels a and b).

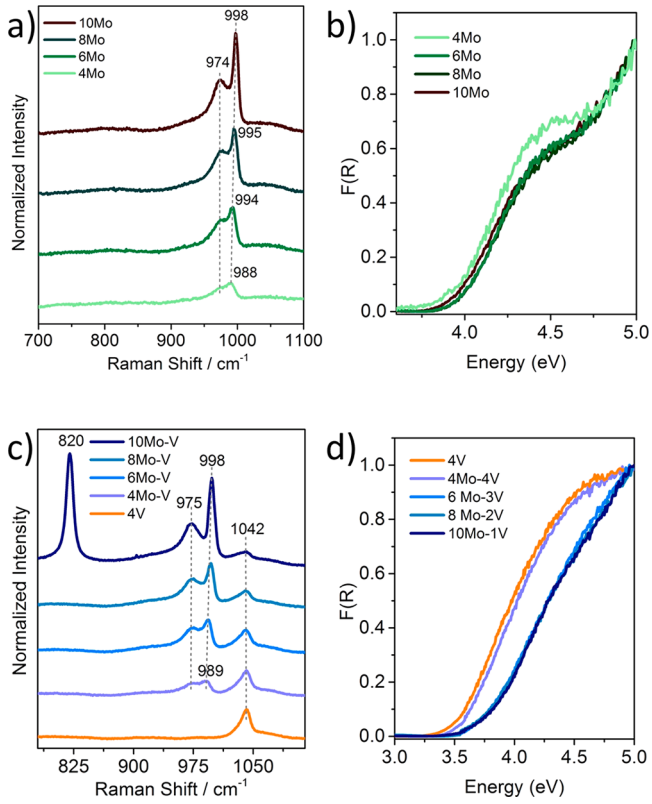

Figure 1. (a) Raman and (b) UV/vis spectra of mMo catalysts, (c) Raman and (d) UV/vis spectra of mMo-nV catalysts; Raman spectra were measured with an excitation wavelength of 532 nm (2.33 eV). Raman spectra in the entire range are shown in Figure S2. UV/vis spectra were normalized to 5 eV, and UV/vis spectra without normalization are shown in Figure S3.

The symmetric O=Mo=O stretching vibration shifts from 988 to 998 cm^{-1} with increasing molybdenum oxide loading (Figure 1a).[41−45] Furthermore, the intensity ratio of the peaks due to symmetric and asymmetric stretching vibrations varies. The shift of the symmetric stretching vibration and the varying intensity ratio might be explained by variations in the lateral interactions of the dioxo species with increasing loading. However, it is not easily understandable why no shift is

DOI: 10.1021/acscatal.9b00326
ACS Catal. 2019, 9, 4875−4886

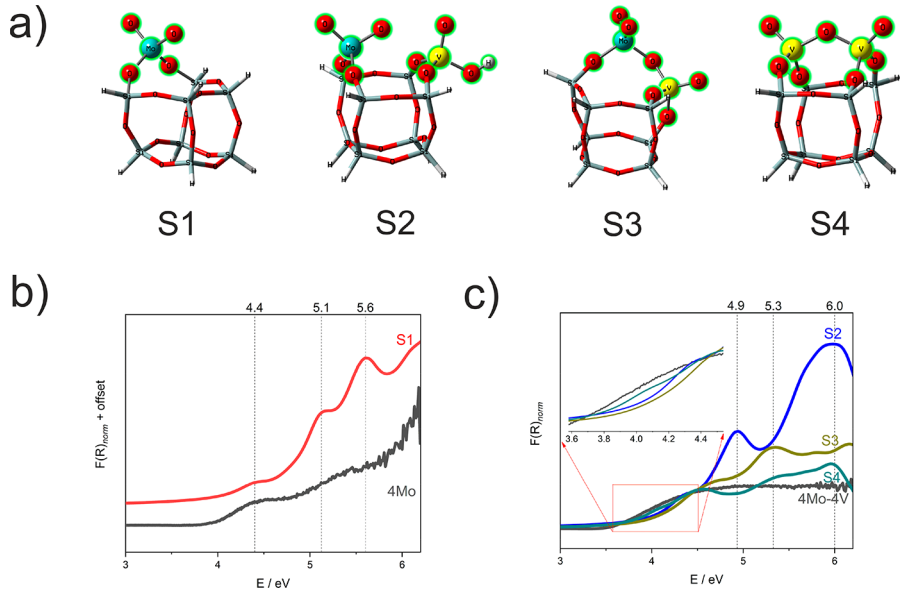

Figure 2. (a) Optimized geometries of the calculated clusters (Table S1) (molybdenum, cyan; vanadium, yellow; oxygen, red; silicon, gray; and hydrogen, light gray); comparison of experimental (black lines) and calculated (colored lines) UV/vis spectra of (b) 4Mo and (c) 4Mo-4V. All spectra are normalized at 4.51 eV (see also not normalized experimental spectra in Figure S3).

observed for the asymmetric stretching vibration at 974 cm^{-1} and why the full width at half-maximum of the bands due to symmetric and asymmetric stretching vibrations is so different. One explanation might be the overlap of the low-frequency band with ν(Mo−O−Si) stretching vibrations expected in the range between 850 and 950 cm^{-1},[41] which might compensate a shift and explains the variable intensity ratio. Another reason will be discussed further below in the analysis of the spectroscopic patterns of the V_xO_y-MoO_x/SiO_2 catalysts by consulting the results of DFT calculations.

With increasing Mo content, very weak peaks at 497 and 607 cm^{-1} gain in intensity (Figure S2a), which might be attributed to symmetric and asymmetric Mo−O−Mo stretching vibrations,[47] related to the occurrence of partial oligomerization. Oligomers may also contribute to the broad low-frequency tail of the Mo═O stretching vibrations in the range between 850 and 970 cm^{-1}.[48] On the other hand, the peaks at 497 and 607 cm^{-1} could also be attributed to D1 and D2 defect modes of cyclic tetra- and trisiloxane rings, respectively, of the amorphous SBA-15, which is considered to be more likely as will be discussed for the V-containing catalysts below.[49]

The UV/vis spectra (Figure 1b) are very similar in shape for all molybdenum oxide loadings, indicating that the coordination sphere of molybdenum does not significantly change in the series. The intensity of the overall spectrum increases with increasing Mo loading (Figure S3a).

In summary, the Raman and UV/vis spectra of the silica-supported molybdenum oxide catalysts are in agreement with the absence of oligomeric Mo oxide species. Dioxo $(Si-O-)_2Mo(=O)_2$ moieties are the predominant surface species. The conclusion is based not only on the Raman results but also on the comparison of the present catalyst series with previously investigated catalysts prepared by the same synthesis technique, which have been additionally characterized by EXAFS, NEXAFS, NMR, and DRIFTS.[11,29]

V_xO_y/SiO_2. The average OH consumption per V for the 4V catalyst is 1.8 (Figure S1, panels c and d), which is in agreement with the formation of surface vanadium oxide species exhibiting a small degree of oligomerization. The structure of surface vanadium oxide species has been discussed controversially based on Raman spectroscopy.[3,50−57] The Raman spectrum (Figure 1c, orange spectrum) shows a maximum at 1042 cm^{-1} with a tail to lower (1025 cm^{-1}) and higher (1070 cm^{-1}) wavenumbers attributed to combinations of V−O−V and V−O−Si (1025 cm^{-1}) as well as V═O and V−O−Si (1050, 1075 cm^{-1}) stretching vibrations based on model calculations.[58] Our previous DFT calculations and simulations of Raman spectra were in agreement with a mixture of monomeric ($VSi_7H_7O_{13}$, $VSi_7H_9O_{13}$, and $VSi_7H_{11}O_{13}$), dimeric ($V_2Si_6H_6O_{14}$ and $V_2Si_{12}H_{12}O_{23}$), trimeric ($V_3Si_5H_5O_{15}$), and tetrameric ($V_4Si_4H_4O_{16}$) model structures, which is also in accordance with recent high-field ^{51}V MAS NMR studies of silica-supported vanadium oxide catalysts.[59] The OH/V ratio in such a model mixture corresponds to 1.4, which is slightly lower compared to the present experimental value of 1.8. Features in the out-of-phase V−O−V stretching vibrations (600−800 cm^{-1}) appear very weak (Figure S2, panel b),[51] which points to the low degree of oligomerization, but due to the weakness of the signals and the strong coupling, Raman spectroscopy alone is not the best method to determine the nature of vanadium oxide surface species.

Also the UV/vis spectrum of 4V is in agreement with a high dispersion of vanadium oxide on the surface of silica and the absence of segregated V_2O_5 nanoparticles (Figure 1d, orange spectrum).

V_xO_y-MoO_x/SiO_2. After introducing V to the Mo-containing catalysts under consumption of the residual OH groups, only 10Mo-1V exhibits a comparable average OH group consumption per V as 4V, while for the remaining three Mo−V catalysts (8Mo-2V, 6Mo-3V, 4Mo-4V) the OH/V value scatters between 0.8 and 1 (Figure S1, panels c and d). The Raman spectrum of 10Mo-1V clearly indicates formation of MoO_3 nanoparticles after grafting of vanadia (peak at 820 cm^{-1} in Figure 1c). This is attributed to the stronger

DOI: 10.1021/acscatal.9b00326
ACS Catal. 2019, 9, 4875−4886

interaction between silica and vanadia compared to the interaction between molybdenum oxide and silica, which in turn apparently forces the dispersed molybdenum oxide to aggregate. The lower value of OH group consumption in 8Mo-2V, 6Mo-3V, and 4Mo-4V is in agreement with an OH deficit due to the preceding coverage of silica by Mo oxide species, which may also lead to the formation of V−O−Mo bonds without consumption of silanol groups. However, the formation of metal−oxygen−metal bonds is not supported by spectroscopy. Raman spectra in the range of M-O-M stretching and bending vibrations provide no clear evidence for the formation of mixed Mo−V oxide species on the SBA-15 support (Figure S2b), which is different from results obtained with alumina-supported Mo−V oxides.[22,60] A band at 771 cm^{-1} has been assigned to V−O−Mo stretches in alumina-supported MoV oxide.[22] Only very weak bands again at the same wavenumbers of 497 and 607 cm^{-1} identical to mMo catalysts (Figure S2, panels a and b) are observed in this range that are most likely originated by defect modes of silica as discussed above for mMo. Moreover, the features do not specifically differ from the spectrum of 4V and become even weaker in the Mo−V catalysts, suggesting that molybdenum oxide species might break V−O−V bonds of vanadium oxide oligomers and lead to the stabilization of single-site (isolated) vanadyl species.

To further analyze any potential vanadia-molybdena interaction in the monolayer, Raman and UV/vis spectra were simulated performing DFT calculations on cluster models that distinguish four simple boundary cases (Figures 2a and S4−S5). A silsesquioxane ($Si_8O_{12}H_8$) cluster was used to represent the silica support.[29−31,58] Figure 2a shows the optimized structures of the generated surface models. The coordinates of the energetically optimized models are given in Table S1. Supported Mo oxide catalysts are represented by one tetrahedral dioxo $(Si{-}O{-})_2Mo(=O)_2$ unit (denoted as model S1). Two simplified options have been considered for the Mo−V catalysts (denoted as models S2 and S3, respectively). Model S2 depicts no direct interaction between surface molybdenum and vanadium oxide species because it contains separated Mo dioxo $(Si{-}O{-})_2Mo(=O)_2$ and $(Si{-}O{-})_2(V{=}O)OH$ units anchored on one silsesquioxane cluster, while model S3 simulates the formation of a Mo−O−V bond. In model S2, a V−OH structure was adopted to balance the cluster. As can be seen in Figures S4 and S5, the V−OH structure does not significantly affect the assignment of the Raman and UV/vis spectra, respectively. The supported vanadium oxide catalyst 4V is represented by the vanadium dimer $(Si{-}O)_2(V{=}O){-}O{-}(V{=}O)(Si{-}O)_2$ (termed as model S4) to simulate V−O−V bridge formation in a cluster of nucleatity two.

The calculated Raman spectrum of the dimeric vanadium oxide cluster (Figures S4, panels a and e) agrees very well with the experimental spectrum (Figures 1c and S2b). The calculated peak maximum is located at 1042 cm^{-1} (exptl: 1042 cm^{-1}) with a tail at lower energy at 1029 cm^{-1} (exptl: 1025 cm^{-1}) and a tail at higher energy at 1074 cm^{-1} (exptl: 1070 cm^{-1}). The calculated modes are in agreement with our previous computational study in which a greater variety of models was included.[58]

The formation of Mo−O−V bonds is also not supported by the Raman spectrum of a mixed Mo−V oxide cluster anchored on silica (model S3). The corresponding calculated Mo−O−V stretching mode occurs at 813 cm^{-1} (Figure S4d). No peak is observed in the experimental spectra in that range (Figures 1c and S2b).

Interestingly, a similar shift of the peak at 989 cm^{-1} to 998 cm^{-1}, which has been attributed to the symmetric O=Mo=O stretching vibration of dioxo $(Si{-}O{-})_2Mo(=O)_2$ species in the pure molybdenum oxide catalysts, is also observed in the experimentally determined spectra of the mixed Mo−V oxide catalysts with increasing molybdenum oxide loading (Figures 1c and S2b). The shift can be explained by referring to the Raman spectrum of model S2. The positions of the calculated asymmetric and symmetric stretching modes of the O=Mo=O moiety in model S1 (at 932 and 980 cm^{-1}, respectively) (Figure S4b) do not move by adding the vanadium oxide species in model S2 (Figure S4c). However, in the case of model S2, an additional vibrational mode at 1007 cm^{-1} appears (Figure S4c), which is assigned to a coupling of the symmetric stretching O=Mo=O mode with the symmetric stretching modes of $Mo{-}(O{-}Si)_2$ and $V{-}(O{-}Si)_2$ (vibrational modes illustrated in Vibrational modes of model S2 at 1007 cm^{-1} in the Supporting Information). Considering insufficient resolution and broadening of the peaks in the experiment, the appearance of the new peak may cause the shift of the band at 989 cm^{-1} to higher wavenumbers with increasing metal oxide loading. The observed shifts, in both the mMo as well as the mMo-nV series, may reflect the vibrational coupling of neighboring isolated metal oxide surface species via the support.

As discussed above, the UV/vis spectra of the dehydrated mMo catalysts show increasing absorption in the high-energy region with increasing Mo loading (see Figure S3a for the not normalized spectra) but only very small changes in the shape (Figure 1b) indicating only small differences in the local coordination of the Mo and O atoms within the series of catalysts, again in agreement with previous studies.[11,29] The edge of the 4Mo-4V spectrum is only slightly blue-shifted compared to the spectrum of the Mo-free 4V catalyst (Figure 1d), which is in accordance with the very similar apparent surface density of V atoms on the two catalysts of 0.7−0.8 V/nm^2 (Table 1). The similarity of the two spectra suggests similar speciation of the vanadium oxide species in the 4V and 4Mo-4V.[31,58] However, the optical edge shifts significantly to higher energy with increasing dilution of V_xO_y with MoO_x although the apparent surface density of vanadium does not decrease very much (Table 1). The spectra of 10Mo-1V, 8Mo-2V, and 6Mo-3V (V/nm^2 ≈ 0.5) resemble very much the spectra of the corresponding V-free Mo catalysts (Figures 1, panels b and d, and S3, panels a and b). The blue shift might be caused by disruption of V−O−V bonds at higher Mo dilution. It should be noted that optical edge energies similar to 4V and no shifts were observed for pure vanadia catalysts supported on SBA-15 prepared in the same way in the range of vanadium-atom-surface-densities between 0.6 and 1.4 V/nm^2.[61] Combined Raman-UV/vis-XAS-DFT analysis demonstrated the presence of a mixture of mono-, di, tri-, and tetramers in such a case.[58]

The calculated UV/vis spectrum of supported Mo oxide species in absence of vanadium oxide species (model S1) reproduces roughly the experimental spectrum of 4Mo with respect to band positions (Figure 2b), justifying the selected model. The calculated spectrum of two independent surface molybdenum and vanadium oxide species (model S2) predicts intense absorption at 4.9 and 6 eV (Figure 2c) mainly related to ligand-to-metal charge transfer involving $Mo(=O)_2$ and

DOI: 10.1021/acscatal.9b00326
ACS Catal. 2019, 9, 4875−4886

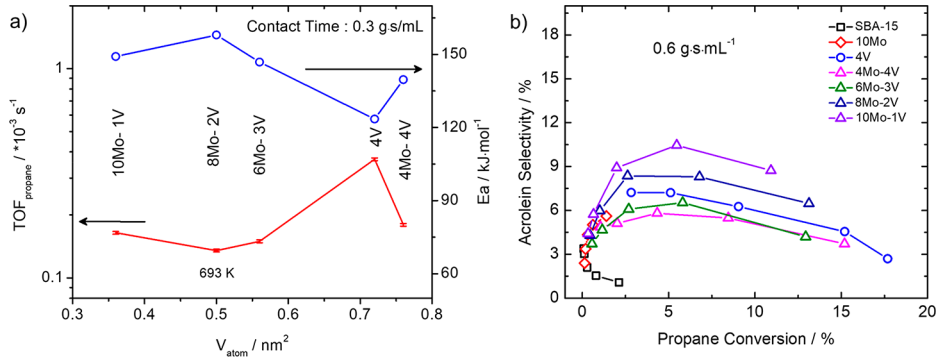

Figure 3. (a) Rate of propane consumption at T = 693 K normalized to the vanadium content of the catalyst (apparent TOF in red including error bar of the measurement) and the apparent activation energy measured in the temperature range of 693−733 K as a function of the apparent V surface density (Arrhenius plots in Figure S7); W/F = 0.3 g s mL^{-1}; feed composition C_3H_8:O_2:N_2 = 10:5:85; (b) selectivity of acrolein as a function of propane conversion measured at different temperatures and constant W/F of 0.6 g s mL^{-1} in a feed composed of C_3H_8:O_2:N_2 = 10:5:85.

V═O moieties, respectively, (Figure S5a) which is not obvious from the experimental spectrum of 4Mo-4V (black line in Figure 2c) that contains Mo and V approximately in a ratio of the one in the models. Concerning the absorption at 6 eV, it should be noted, however, that the reliability of the UV/vis measurements at energies higher than 5 eV is limited due to the optical properties of the diffuse reflectance accessory.[62] The spectrum of model S3 that contains a Mo−O−V bond exhibits an absorption band at 5.3 eV related to the Mo−O—V moiety (Figure S5b), which is again missing in the experimental spectrum of 4Mo-4V. The finding confirms the lacking evidence for Mo−O−V bonds by Raman spectroscopy. The vanadium-only structure (model S4) clearly shows a shift of the edge position to lower energy compared to the simulated spectrum of model S2 that contains a single vandyl site, which matches the experimental spectrum of 4Mo-4V (inset in Figure 2c), indicating the presence of V−O—V moieties in both 4V and 4Mo-4V catalysts.[63,64] The calculation result is also in agreement with previous studies where a red shift of the absorption spectra has been predicted with an increasing degree of oligomerization and in particular upon the presence of V−OH terminations.[31]

In summary, the UV/vis spectra of 4V and 4Mo-4V suggest similarities in the coordination of vanadium oxide species in the two catalysts and the presence of V−O−V bonds. TD-DFT calculations do not support the formation of Mo−O−V moieties in the 4Mo-4V catalyst in agreement with Raman spectroscopy. The progressive dilution of vanadium oxide species with molybdenum oxide in 6Mo-3V, 8Mo-2V, and 10Mo-1V appears to disrupt vanadium oxide ensembles, and the formation of vanadyl single-sites is reflected in a blue-shift of the absorption edge (Figure 1d and Figure 2c).

Oxidation of Propane. All catalysts have been studied in the oxidative dehydrogenation of propane (ODP). Propane and oxygen consumption as a function of temperature are shown in Figure S6. Oxygen conversion does not exceed 80% at the highest reaction temperature and W/F = 0.6 g s mL^{-1} for the most active catalyst 4V. The rate of propane consumption normalized to the V content as a function of the apparent V surface density is presented in Figure 3a. Molybdenum oxide supported on silica shows very low catalytic activity at the applied reaction temperatures.[29] The catalysts are therefore not included in Figure 3a. In previous studies a synergistic effect between molybdenum and vanadium oxide has been observed.[15,19,20,22,60,65] In contrast, in the present work the Mo-free 4V reference catalyst exhibits the highest activity (Figure 3a). The normalized rate (apparent TOF) is comparable to results reported for silica-supported vanadium oxide before.[66] The addition of molybdenum oxide appears to retard the reaction, which is also reflected in an increase in the apparent activation energy compared to 4V (Figure 3a and S7). At comparable conversion, the selectivity to propylene decreases with increasing Mo content (Figure S8, panels a−c). This occurs particularly because acrolein, which is detected as an additional reaction product of partial oxidation (Figures 3b and S8, panels d−f), is increasingly formed with increasing Mo loading. The selectivity toward carbon dioxide is similar at comparable conversion among all Mo−V catalysts (Figure S8, panels g−i), while the selectivity to carbon monoxide increases with increasing Mo content (Figure S8, panels j−l). This suggests that CO is at least in part a product of consecutive decarbonylation of acrolein.[10] The pure vanadium oxide catalyst shows an intermediate selectivity to acrolein. Acrolein is also formed in absence of vanadium over 10Mo, but the selectivity seems to level off at the maximum conversion of about 2%, whereas the selectivity increases further over 10Mo-1V, reaching a maximum of about 10% at 5% conversion (Figure 3b). Acrolein formation is therefore mainly attributed to V-containing surface species. Oxygen activation on isolated surface vanadyl sites under formation of peroxovanate species has been proposed to be responsible for acrolein formation by theory.[67] Peroxovanadate species are supposed to oxidize propylene in a consecutive reaction to propylene oxide, which is further converted into acrolein and acetone. The higher abundance of electrophilic oxygen species under steady state conditions due to limited redox properties of a monolayer vanadium oxide catalyst has been postulated to be responsible for extensive undesired total combustion to CO and CO_2 via acrolein as an intermediate.[4,10,68] The stabilization of single vanadyl sites by dilution with molybdenum oxide is apparently reflected in increasing acrolein selectivity with decreasing V-content in the mixed metal oxide catalysts. The similar acrolein selectivity over the V-free molybdenum oxide catalysts might suggest that also over supported molybdenum oxide catalysts acrolein is formed on the present isolated dioxo $(Si-O-)_2Mo(=O)_2$ species, albeit with lower rates.

In summary, the rate of propane oxidation normalized to the V content (apparent TOF) decreases upon dilution of

DOI: 10.1021/acscatal.9b00326
ACS Catal. 2019, 9, 4875−4886

supported vanadium oxide with molybdenum oxide species. In accordance with Raman and UV/vis spectroscopy, this is attributed to the breaking of M−O−M bonds. The finding is in accordance with the observation that the specific rate of propane oxidation over supported vanadium oxide catalysts increases with increasing loading, i.e., supposedly due to an increased degree of oligomerization.[69,70]

We postulate that acrolein formation by consecutive oxidation of propylene over mixed Mo−V oxide catalysts is not related to the presence of molybdenum oxide in the catalysts but to the presence of isolated single-site metal oxide species, either MoO_x (low activity) or VO_x (high activity), with limited capability to reduce oxygen fast to nucleophilic O^{2-}.

Redox Properties. The redox properties of the catalysts have been studied by temperature-programmed reduction with hydrogen (H_2-TPR), time-resolved diffuse reflectance UV/vis spectroscopy, and EPR. The temperature profiles of hydrogen consumption reveal a slight shift of the maximum to higher reduction temperatures for the mixed metal oxide catalysts compared to 4V and 10Mo (Figure S9) in agreement with observations previously reported for related catalysts.[21,71] Hydrogen consumption (Table S2) indicates formation of V^{4+} and V^{3+} in 4V and Mo^{3+} in 10Mo, respectively. Expected hydrogen consumption in the entire temperature range (up to 1250 K) of the H_2-TPR experiment for the mixed metal oxide catalysts calculated based on the metal content and normalized to the hydrogen consumption in 4V on the one side and 10Mo on the other side is plotted in Figure S10 (dotted line) versus the measured hydrogen consumption (data points). Only 10Mo-1V shows a higher average degree of reduction, which is in agreement with the presence of segregated nanocrystalline MoO_3 in this catalyst as observed by Raman spectroscopy (Figure 1c). All other catalysts exhibit a slightly lower degree of reduction than expected, which indicates that higher oxidation states are stabilized in the mixed metal oxides during reduction with hydrogen.

More insight is provided by an investigation of the overall redox dynamics applying time-resolved in situ UV/vis spectroscopy in oxygen and propane according to a methodology described in the literature.[27,72,73] The Kubelka−Munk function recorded at 700 nm (1.77 eV) during switching the gas feed from O_2/He to C_3H_8/He at 693 K increases with time, which becomes apparent by plotting the change of $F(R)$ with respect to the initial value after in situ calcination of the catalyst $\Delta F(R)$ as a function of time (Figure S11). An increase of $F(R)$ indicates that the catalysts are being reduced under the assumption that the scattering coefficient S remains constant and mass transport limitations are not significant. These two assumptions are most likely justified in case of monolayer catalysts. Since under propane oxidation condition the catalyst will not possess a high reduction degree due to the presence of oxygen, the initial reduction rate in C_3H_8 is applied as an indicator of the redox properties. Assuming apparent zero reaction order, the rate of reduction k_{red} was estimated directly from the slope determined in the range of the dotted lines in Figure S11.

The reduction rate is the lowest for 10Mo and the highest for 4V but for the mixed metal oxide catalysts 10Mo-1V, 8Mo-2V, and 6Mo-3V independent of the V content (Figure 4). The constant reduction rate indicates that the nature of the reducible metal oxide species does not change among these three catalysts. This observation is in agreement with the

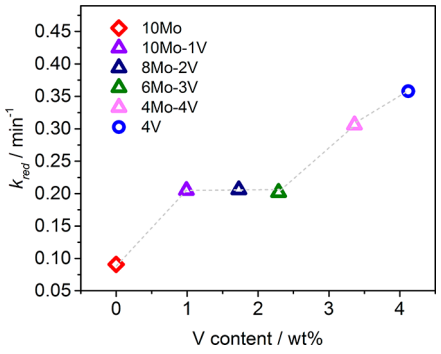

Figure 4. Rate of reduction k_{red} at 693 K as determined based on the change in F(R) by switching the flow from O_2/He (20/80) to C_3H_8/He (20/80) (see Figure S11 for raw data) as a function of the V content. The dotted line was added to guide the eye.

similarity of the UV/vis spectra that suggest the predominant presence of isolated monomeric vanadium and molybdenum oxide species (single sites). The V and Mo single sites present in these three catalysts are apparently not affected with respect to reducibility due to the largely absence of mutual interaction. In contrast, more M−O−M bonds are present in 4Mo-4V and 4V. Moreover, the UV/vis spectra of both, 4Mo-4V and 4V, definitely reveal a similar degree of oligomerization of the vanadium oxide species in these two catalysts, which is reflected in an improved reducibility underlining the limited performance of single sites in facilitating redox reactions. Indeed, the overall rate of reduction decreases with increasing energy of the optical edge (Figures 5a and S12).

Moreover, the rate of propane consumption correlates linearly with the rate of reduction normalized to the total metal content (Figure 5b) establishing a link between redox properties and catalytic activity.

After reduction, the reoxidation has been studied by switching the feed to a mixture of oxygen and helium (O_2/He = 20/80) at 693 K. As shown in Figure S13, the initial reoxidation rates for the Mo−V catalysts are lower compared to 4V. But in general, the rate constants of reoxidation are by 1 order of magnitude higher compared to the rate constants of reduction revealing fast reoxidation as frequently observed over vanadium oxide-based catalysts.

The EPR spectra of 4V and 4Mo-4V are presented in Figure S14. In the hydrated catalysts, V^{4+} is detected in both 4V and 4Mo-4V as shown by the characteristic hyperfine structure due to the coupling of an unpaired electron to ^{51}V with a nuclear spin of 7/2. A fit of the spectra with the EasySpin program[74] yielded the g values of $g_{11} \approx g_{22} \approx 1.98$ and $g_{33} \approx 1.93$ and principal values of the hyperfine tensor of $A_{11} \approx 200$ MHz, $A_{22} \approx 214$ MHz, and $A_{33} \approx 546$ MHz (approximate axial symmetry) in agreement with the literature on supported vanadium oxides on SBA-15.[75] After calcination under O_2 atmosphere, the V^{4+} in 4V disappeared almost completely, while in 4Mo-4V, traces of V^{4+} can still be detected (Figure S14). The g value of the remaining signal is ~1.96, which might be caused by interacting V^{4+} species.[76] The hyperfine structure of V^{4+} becomes visible again upon treating the samples in 100 mbar propane, yet the signal intensity is lower than in the hydrated catalysts.

In summary, H_2-TPR, EPR, and UV/vis spectroscopy experiments demonstrate that the addition of molybdenum oxide decreases the overall rate of reduction of oxidized MO_x species (M = V,Mo) in silica-supported mixed Mo−V oxide

DOI: 10.1021/acscatal.9b00326
ACS Catal. 2019, 9, 4875−4886

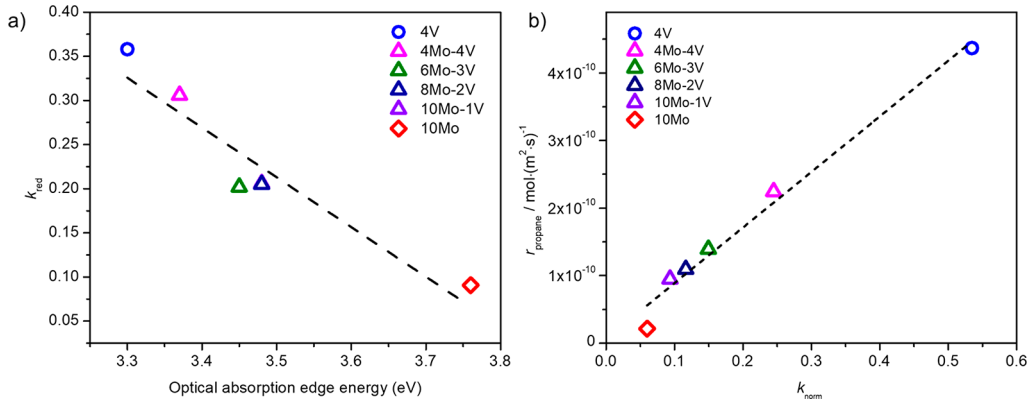

Figure 5. (a) Rate of reduction k_{red} at 693 K as determined based on the change in $F(R)$ by switching the flow from O_2/He (20/80) to C_3H_8/He (20/80) (see Figure S11 for raw data) as a function of the optical edge energy estimated from the UV/vis spectra (see Figure S12 for determination of the optical edge); (b) rate of propane consumption in the oxidative dehydrogenation of propane at 673 K, W/F = 0.3 g s mL^{-1}, and in a feed composed of C_3H_8:O_2:N_2 = 10:5:85 versus rate constant of reduction in propane normalized to the total metal content.

catalysts compared to vanadium oxide supported on silica, and it decreases also the rate of reoxidation of the corresponding reduced species by oxygen. Furthermore, the linear relationship in Figure 5b reveals that the overall propane consumption rate in the oxidative dehydrogenation of propane is higher for the catalysts that exhibit higher k_{Mo-V}. Catalyst 4V shows the highest and 10Mo the lowest rates in reduction with propane and oxidative dehydrogenation of propane, respectively. Generally, the mixed metal oxide catalysts exhibit lower rate constants of reduction compared to the vanadia catalyst due to the presence of isolated single-site metal oxide species.

CONCLUSIONS

In this work, the interaction between molybdenum and vanadium oxide species on the surface of mesostructured silica SBA-15 has been studied by synthesis of a series of near-monolayer catalysts that contain Mo and V in a variable ratio between 10 and 1. Spectroscopic analysis by Raman and UV/vis spectroscopy in combination with DFT calculations provide no clear evidence of the formation of Mo−O−V bonds in the mixed metal oxide catalysts, which is in contrast to previous studies of mixed Mo−V oxide catalysts supported on other supports.

In the pure silica-supported vanadium oxide catalyst and in the mixed catalyst with the highest vanadium content, oligomeric vanadium oxide species exhibiting a nuclearity of 2−4 occur, while the pure molybdenum oxide catalysts predominantly contain isolated dioxo $(Si-O-)_2Mo(=O)_2$ species. With an increasing fraction of molybdenum oxide in the monolayer (Mo/V > 1), V−O−V bonds in the vanadia surface oligomers and, if present, Mo−O−V bonds in mixed species are disrupted and single $(Si-O-)_3V(=O)$ sites are formed surrounded by diluting (because catalytically less active) dioxo $(Si-O-)_2Mo(=O)_2$ species as evidenced by UV/vis and Raman spectroscopy.

These single metal oxide sites exhibit no mutual interaction, which is manifested in an almost constant rate of reduction irrespective of the Mo/V ratio. The rate of reduction for the single-site catalysts is much lower compared to reduction rate of catalysts that contain oligomeric vanadium oxide species. The rate of reduction in propane correlates with the rate of propane oxidation. The result indicates that oligomeric species in a monolayer facilitate both, C−H activation and the oxidation of alkanes most likely due to improved oxygen activation.

The retarded redox properties of isolated Mo or V oxide species in single-site catalysts promote a higher abundance of electrophilic oxygen species under steady state conditions, which is reflected in an improved selectivity toward acrolein. The finding is in agreement with site-isolation concepts postulated for complex metal oxides where a structural and surface analysis is much more complicated.[77]

The present model system may be used to perform more experiments in the future to resolve apparent contradictions concerning the reactivity of single sites versus larger metal oxide clusters in other oxidation reactions.[3] The current example shows that the catalytic properties as consequence of the local electronic structure are by no means proportional to the loading or the dilution factor. Therefore, it is not possible to simply vary the catalytic properties of such supported systems by varying their composition, which might be the reason for contradicting results in standard experimentation. The results are governed by oxide−oxide interactions including the support with implications on catalyst optimization strategies based on big data and machine learning. Apparently, nonlinear effects are critical in catalyst tuning that can, however, be well seen from the redox properties determined through operando experimentation.

ASSOCIATED CONTENT

Supporting Information

The Supporting Information is available free of charge on the ACS Publications website at DOI: 10.1021/acscatal.9b00326.

Experimental IR, Raman and UV/vis spectra of the catalysts; calculated Raman spectra of model S1, S2, S3, and S4 with selected vibrational modes; coordinates of optimized Mo and MoV clusters; illustration of electron density differences between ground and excited state related to the selected transitions indicated in model S2 and S3; propane and oxygen conversion as a function of reaction temperature at the highest W/F = 0.6 g s mL^{-1}; Arrhenius plots; selectivity (propene, acrolein, CO_2, and CO) as a function of propane conversion under different temperature and contact time; hydrogen consumption profile and correlation between measured and calculated reduction degree during TPR experiment; UV/vis

DOI: 10.1021/acscatal.9b00326
ACS Catal. 2019, 9, 4875−4886

transient study under C_3H_8/He and O_2/He; determination of optical absorption edge; EPR spectra of 4V and 4Mo-4V catalysts after different pretreatments (PDF)
Vibrational modes of model S1 at 179 cm^{-1} (AVI)
Vibrational modes of model S1 at 334 cm^{-1} (AVI)
Vibrational modes of model S1 at 924 cm^{-1} (AVI)
Vibrational modes of model S1 at 932 cm^{-1} (AVI)
Vibrational modes of model S1 at 980 cm^{-1} (AVI)
Vibrational modes of model S2 at 932 cm^{-1} (AVI)
Vibrational modes of model S2 at 980 cm^{-1} (AVI)
Vibrational modes of model S2 at 1007 cm^{-1} (AVI)
Vibrational modes of model S2 at 1040 cm^{-1} (AVI)
Vibrational modes of model S3 at 813 cm^{-1} (AVI)
Vibrational modes of model S3 at 934 cm^{-1} (AVI)
Vibrational modes of model S3 at 980 cm^{-1} (AVI)
Vibrational modes of model S3 at 1035 cm^{-1} (AVI)
Vibrational modes of model S4 at 956 cm^{-1} (AVI)
Vibrational modes of model S4 at 994 cm^{-1} (AVI)
Vibrational modes of model S4 at 1029 cm^{-1} (AVI)
Vibrational modes of model S4 at 1042 cm^{-1} (AVI)
Vibrational modes of model S4 at 1074 cm^{-1} (AVI)

AUTHOR INFORMATION

Corresponding Author

*Tel.: +49 30 8413 4457, E-mail: trunschke@fhi-berlin.mpg.de.

ORCID

Yuanqing Wang: 0000-0002-1332-7956
Annette Trunschke: 0000-0003-2869-0181

Present Addresses

[‖]T.F.: Department of Chemical and Biomolecular Engineering, University of California at Berkeley, Berkeley, CA 94720, USA.
[⊥]T.F. moved to the following address: Department of Chemical and Biomolecular Engineering, University of California at Berkeley, Berkeley, CA 94720, USA.

Author Contributions

The manuscript was written through contributions of all authors.

Notes

The authors declare no competing financial interest.

ACKNOWLEDGMENTS

The work was conducted in the framework of the BasCat collaboration between BASF SE, TU Berlin, FHI, and the German Research Foundation, cluster of excellence "Unified Concepts in Catalysis" (UniCat www.unicat.tu-berlin.de). We thank Dr. Pierre Kube for his support in catalyst testing, Maike Hashagen for surface area determination, Dr. Olaf Timpe for chemical analysis by XRF, Jasmin Allan for thermal analysis, and the Computer Support Group of the Fritz-Haber-Institut for providing computational resources.

REFERENCES

(1) Grant, J. T.; Venegas, J. M.; McDermott, W. P.; Hermans, I. Aerobic Oxidations of Light Alkanes over Solid Metal Oxide Catalysts. *Chem. Rev.* **2018**, *118*, 2769−2815.
(2) Chieregato, A.; López Nieto, J. M.; Cavani, F. Mixed-oxide catalysts with vanadium as the key element for gas-phase reactions. *Coord. Chem. Rev.* **2015**, *301*−*302*, 3−23.
(3) Wachs, I. E. Catalysis science of supported vanadium oxide catalysts. *Dalton Transactions* **2013**, *42*, 11762−11769.
(4) Schlögl, R. Active Sites for Propane Oxidation: Some Generic Considerations. *Top. Catal.* **2011**, *54*, 627−638.
(5) Ishikawa, S.; Ueda, W. Microporous crystalline Mo-V mixed oxides for selective oxidations. *Catal. Sci. Technol.* **2016**, *6*, 617−629.
(6) Amakawa, K.; Kolen'ko, Y. V.; Villa, A.; Schuster, M. E.; Csepei, L.-I.; Weinberg, G.; Wrabetz, S.; Naumann d'Alnoncourt, R.; Girgsdies, F.; Prati, L.; Schlögl, R.; Trunschke, A. Multifunctionality of Crystalline MoV(TeNb) M1 Oxide Catalysts in Selective Oxidation of Propane and Benzyl Alcohol. *ACS Catal.* **2013**, *3*, 1103−1113.
(7) Trunschke, A.; Noack, J.; Trojanov, S.; Girgsdies, F.; Lunkenbein, T.; Pfeifer, V.; Hävecker, M.; Kube, P.; Sprung, C.; Rosowski, F.; Schlögl, R. The Impact of the Bulk Structure on Surface Dynamics of Complex Mo−V-based Oxide Catalysts. *ACS Catal.* **2017**, *7*, 3061−3071.
(8) Heine, C.; Hävecker, M.; Sanchez-Sanchez, M.; Trunschke, A.; Schlögl, R.; Eichelbaum, M. Work Function, Band Bending, and Microwave Conductivity Studies on the Selective Alkane Oxidation Catalyst MoVTeNb Oxide (Orthorhombic M1 Phase) under Operation Conditions. *J. Phys. Chem. C* **2013**, *117*, 26988−26997.
(9) Hävecker, M.; Wrabetz, S.; Kröhnert, J.; Csepei, L.-I.; Naumann d'Alnoncourt, R.; Kolen'ko, Y. V.; Girgsdies, F.; Schlögl, R.; Trunschke, A. Surface chemistry of phase-pure M1MoVTeNb oxide during operation in selective oxidation of propane to acrylic acid. *J. Catal.* **2012**, *285*, 48−60.
(10) Kube, P.; Frank, B.; Schlögl, R.; Trunschke, A. Isotope Studies in Oxidation of Propane over Vanadium Oxide. *ChemCatChem* **2017**, *9*, 3446−3455.
(11) Amakawa, K.; Sun, L.; Guo, C.; Hävecker, M.; Kube, P.; Wachs, I. E.; Lwin, S.; Frenkel, A. I.; Patlolla, A.; Hermann, K.; Schlögl, R.; Trunschke, A. How Strain Affects the Reactivity of Surface Metal Oxide Catalysts. *Angew. Chem., Int. Ed.* **2013**, *52*, 13553−13557.
(12) Tsilomelekis, G.; Boghosian, S. An operando Raman study of molecular structure and reactivity of molybdenum(vi) oxide supported on anatase for the oxidative dehydrogenation of ethane. *Phys. Chem. Chem. Phys.* **2012**, *14*, 2216−2228.
(13) Fu, G.; Xu, X.; Lu, X.; Wan, H. L. Mechanisms of initial propane activation on molybdenum oxides: A density functional theory study. *J. Phys. Chem. B* **2005**, *109*, 6416−6421.
(14) Chen, K.; Xie, S.; Bell, A. T.; Iglesia, E. Structure and Properties of Oxidative Dehydrogenation Catalysts Based on MoO3/Al2O3. *J. Catal.* **2001**, *198*, 232−242.
(15) Meunier, F. C.; Yasmeen, A.; Ross, J. R. H. Oxidative dehydrogenation of propane over molybdenum-containing catalysts. *Catal. Today* **1997**, *37*, 33−42.
(16) Chen, K.; Bell, A. T.; Iglesia, E. Kinetics and Mechanism of Oxidative Dehydrogenation of Propane on Vanadium, Molybdenum, and Tungsten Oxides. *J. Phys. Chem. B* **2000**, *104*, 1292−1299.
(17) Cavani, F.; Ballarini, N.; Cericola, A. Oxidative dehydrogenation of ethane and propane: How far from commercial implementation? *Catal. Today* **2007**, *127*, 113−131.
(18) Haddad, N.; Bordes-Richard, E.; Barama, A. MoOx-based catalysts for the oxidative dehydrogenation (ODH) of ethane to ethylene: Influence of vanadium and phosphorus on physicochemical and catalytic properties. *Catal. Today* **2009**, *142*, 215−219.
(19) Solsona, B.; Dejoz, A.; Garcia, T.; Concepcion, P.; Nieto, J. M. L.; Vazquez, M. I.; Navarro, M. T. Molybdenum-vanadium supported on mesoporous alumina catalysts for the oxidative dehydrogenation of ethane. *Catal. Today* **2006**, *117*, 228−233.
(20) Mitra, B.; Wachs, I. E.; Deo, G. Promotion of the propane ODH reaction over supported V2O5/Al2O3 catalyst with secondary surface metal oxide additives. *J. Catal.* **2006**, *240*, 151−159.
(21) Chary, K. V. R.; Kumar, C. P.; Rajiah, T.; Srikanth, C. S. Dispersion and reactivity of monolayer vanadium oxide catalysts supported on zirconia: The influence of molybdena addition. *J. Mol. Catal. A: Chem.* **2006**, *258*, 313−319.
(22) Yang, S.; Iglesia, E.; Bell, A. T. Oxidative Dehydrogenation of Propane over V2O5/MoO3/Al2O3 and V2O5/Cr2O3/Al2O3:

DOI: 10.1021/acscatal.9b00326
ACS Catal. 2019, 9, 4875−4886

Structural Characterization and Catalytic Function. *J. Phys. Chem. B* **2005**, *109*, 8987−9000.
(23) Kholyavenko, K. M.; Öhlman, G.; Schnabel, K.; Hanke, W.; Minow, G.; Fiebig, W.; Gorokhovatskii, Y. B.; Baryshevskaya, I. M.; Rozhkova, E. V.; Yaremenko, E. I. Catalytic properties of grafted vanadium and molybdenum oxide catalysts in oxidations of propylene and propane. *Kataliz i Katalizatory* **1979**, *17*, 25−7.
(24) Artiglia, L.; Agnoli, S.; Granozzi, G. Vanadium oxide nanostructures on another oxide: The viewpoint from model catalysts studies. *Coord. Chem. Rev.* **2015**, *301*−*302*, 106−122.
(25) Hamilton, N.; Wolfram, T.; Tzolova Müller, G.; Hävecker, M.; Kröhnert, J.; Carrero, C.; Schomäcker, R.; Trunschke, A.; Schlögl, R. Topology of silica supported vanadium-titanium oxide catalysts for oxidative dehydrogenation of propane. *Catal. Sci. Technol.* **2012**, *2*, 1346−1359.
(26) Amakawa, K.; Wrabetz, S.; Kröhnert, J.; Tzolova-Müller, G.; Schlögl, R.; Trunschke, A. In Situ Generation of Active Sites in Olefin Metathesis. *J. Am. Chem. Soc.* **2012**, *134*, 11462−11473.
(27) Ovsitser, O.; Cherian, M.; Brückner, A.; Kondratenko, E. V. Dynamics of redox behavior of nano-sized VOx species over Ti-Si-MCM-41 from time-resolved in situ UV/Vis analysis. *J. Catal.* **2009**, *265*, 8−18.
(28) Sanchez, C.; Livage, J.; Launay, J. P.; Fournier, M.; Jeannin, Y. Electron delocalization in mixed-valence molybdenum polyanions. *J. Am. Chem. Soc.* **1982**, *104*, 3194−3202.
(29) Guo, C. S.; Hermann, K.; Hävecker, M.; Thielemann, J. P.; Kube, P.; Gregoriades, L. J.; Trunschke, A.; Sauer, J.; Schlögl, R. Structural Analysis of Silica-Supported Molybdena Based on X-ray Spectroscopy: Quantum Theory and Experiment. *J. Phys. Chem. C* **2011**, *115*, 15449−15458.
(30) Guo, C. S.; Hermann, K.; Hävecker, M.; Trunschke, A.; Schlögl, R. Silica-Supported Titania Species: Structural Analysis from Quantum Theory and X-ray Spectroscopy. *J. Phys. Chem. C* **2012**, *116*, 22449−22457.
(31) Klokishner, S.; Reu, O.; Tzolova-Müller, G.; Schlögl, R.; Trunschke, A. Apparent Absorption Spectra of Silica Supported Vanadium−Titanium Oxide Catalysts: Experimental Study and Modeling. *J. Phys. Chem. C* **2014**, *118*, 14677−14691.
(32) Frisch, M. J.; Trucks, G. W.; Schlegel, H. B.; Scuseria, G. E.; Robb, M. A.; Cheeseman, J. R.; Scalmani, G.; Barone, V.; Mennucci, B.; Petersson, G. A.; Nakatsuji, H.; Caricato, M.; Li, X.; Hratchian, H. P.; Izmaylov, A. F.; Bloino, J.; Zheng, G.; Sonnenberg, J. L.; Hada, M.; Ehara, M.; Toyota, K.; Fukuda, R.; Hasegawa, J.; Ishida, M.; Nakajima, T.; Honda, Y.; Kitao, O.; Nakai, H.; Vreven, T.; Montgomery, J. A.; Peralta, J. E.; Ogliaro, F.; Bearpark, M.; Heyd, J. J.; Brothers, E.; Kudin, K. N.; Staroverov, V. N.; Kobayashi, R.; Normand, J.; Raghavachari, K.; Rendell, A.; Burant, J. C.; Iyengar, S. S.; Tomasi, J.; Cossi, M.; Rega, N.; Millam, J. M.; Klene, M.; Knox, J. E.; Cross, J. B.; Bakken, V.; Adamo, C.; Jaramillo, J.; Gomperts, R.; Stratmann, R. E.; Yazyev, O.; Austin, A. J.; Cammi, R.; Pomelli, C.; Ochterski, J. W.; Martin, R. L.; Morokuma, K.; Zakrzewski, V. G.; Voth, G. A.; Salvador, P.; Dannenberg, J. J.; Dapprich, S.; Daniels, A. D.; Farkas; Foresman, J. B.; Ortiz, J. V.; Cioslowski, J.; Fox, D. J. *Gaussian 09*, revision D.01; Wallingford, CT, 2009.
(33) Grimme, S.; Ehrlich, S.; Goerigk, L. Effect of the damping function in dispersion corrected density functional theory. *J. Comput. Chem.* **2011**, *32*, 1456−1465.
(34) Hay, P. J.; Wadt, W. R. Ab initio effective core potentials for molecular calculations. *J. Chem. Phys.* **1985**, *82*, 270−283.
(35) Wadt, W. R.; Hay, P. J. Ab initio effective core potentials for molecular calculations. Potentials for main group elements Na to Bi. *J. Chem. Phys.* **1985**, *82*, 284−298.
(36) Hay, P. J.; Wadt, W. R. Ab initio effective core potentials for molecular calculations. Potentials for K to Au including the outermost core orbitals. *J. Chem. Phys.* **1985**, *82*, 299−310.
(37) Bauernschmitt, R.; Ahlrichs, R. Treatment of electronic excitations within the adiabatic approximation of time dependent density functional theory. *Chem. Phys. Lett.* **1996**, *256*, 454−464.
(38) Döbler, J.; Pritzsche, M.; Sauer, J. Vibrations of Silica Supported Vanadia: Variation with Particle Size and Local Surface Structure. *J. Phys. Chem. C* **2009**, *113*, 12454−12464.
(39) Guesmi, H.; Grybos, R.; Handzlik, J.; Tielens, F. Characterization of molybdenum monomeric oxide species supported on hydroxylated silica: a DFT study. *Phys. Chem. Chem. Phys.* **2014**, *16*, 18253−18260.
(40) Amakawa, K.; Kröhnert, J.; Wrabetz, S.; Frank, B.; Hemmann, F.; Jäger, C.; Schlögl, R.; Trunschke, A. Active Sites in Olefin Metathesis over Supported Molybdena Catalysts. *ChemCatChem* **2015**, *7*, 4059−4065.
(41) Handzlik, J.; Ogonowski, J. Structure of Isolated Molybdenum-(VI) and Molybdenum(IV) Oxide Species on Silica: Periodic and Cluster DFT Studies. *J. Phys. Chem. C* **2012**, *116*, 5571−5584.
(42) Chempath, S.; Zhang, Y.; Bell, A. T. DFT Studies of the Structure and Vibrational Spectra of Isolated Molybdena Species Supported on Silica. *J. Phys. Chem. C* **2007**, *111*, 1291−1298.
(43) Lee, E. L.; Wachs, I. E. In Situ Spectroscopic Investigation of the Molecular and Electronic Structures of SiO2 Supported Surface Metal Oxides. *J. Phys. Chem. C* **2007**, *111*, 14410−14425.
(44) Lee, E. L.; Wachs, I. E. Molecular Design and In Situ Spectroscopic Investigation of Multilayered Supported M1Ox/M2Ox/SiO2 Catalysts. *J. Phys. Chem. C* **2008**, *112*, 20418−20428.
(45) Gregoriades, L. J.; Döbler, J.; Sauer, J. Oxidation of Methanol to Formaldehyde on Silica-Supported Molybdena: Density Functional Theory Study on Models of Mononuclear Sites. *J. Phys. Chem. C* **2010**, *114*, 2967−2979.
(46) Radhakrishnan, R.; Reed, C.; Oyama, S. T.; Seman, M.; Kondo, J. N.; Domen, K.; Ohminami, Y.; Asakura, K. Variability in the structure of supported MoO3 catalysts: Studies using Raman and X-ray absorption spectroscopy with ab initio calculations. *J. Phys. Chem. B* **2001**, *105*, 8519−8530.
(47) Tian, H.; Roberts, C. A.; Wachs, I. E. Molecular Structural Determination of Molybdena in Different Environments: Aqueous Solutions, Bulk Mixed Oxides, and Supported MoO3 Catalysts. *J. Phys. Chem. C* **2010**, *114*, 14110−14120.
(48) Marianski, M.; Seo, J.; Mucha, E.; Thomas, D. A.; Jung, S.; Schloegl, R.; Meijer, G.; Trunschke, A.; von Helden, G. Structural Characterization of Molybdenum Oxide Nanoclusters Using Ion Mobility Spectrometry-Mass Spectrometry and Infrared Action Spectroscopy. *J. Phys. Chem. C* **2019**, *123*, 7845−7853.
(49) Brinker, C. J.; Kirkpatrick, R. J.; Tallant, D. R.; Bunker, B. C.; Montez, B. NMR confirmation of strained "defects" in amorphous silica. *J. Non-Cryst. Solids* **1988**, *99*, 418−428.
(50) Lewandowska, A. E.; Calatayud, M.; Tielens, F.; Bañares, M. A. Hydration Dynamics for Vanadia/Titania Catalysts at High Loading: A Combined Theoretical and Experimental Study. *J. Phys. Chem. C* **2013**, *117*, 25535−25544.
(51) Magg, N.; Immaraporn, B.; Giorgi, J. B.; Schroeder, T.; Bäumer, M.; Döbler, J.; Wu, Z.; Kondratenko, E.; Cherian, M.; Baerns, M.; Stair, P. C.; Sauer, J.; Freund, H.-J. Vibrational spectra of alumina- and silica-supported vanadia revisited: An experimental and theoretical model catalyst study. *J. Catal.* **2004**, *226*, 88−100.
(52) Moisii, C.; van de Burgt, L. J.; Stiegman, A. E. Resonance Raman Spectroscopy of Discrete Silica-Supported Vanadium Oxide. *Chem. Mater.* **2008**, *20*, 3927−3935.
(53) Moncada, J.; Adams, W. R.; Thakur, R.; Julin, M.; Carrero, C. A. Developing a Raman Spectrokinetic Approach To Gain Insights into the Structure−Reactivity Relationship of Supported Metal Oxide Catalysts. *ACS Catal.* **2018**, *8*, 8976−8986.
(54) Stair, P. C. The Application of UV Raman Spectroscopy for the Characterization of Catalysts and Catalytic Reactions. In *Advances in Catalysis*; Gates, B. C.; Knozinger, H., Eds.; Elsevier Academic Press Inc: San Diego, 2007; Vol. *51*, pp 75−98.
(55) Waleska, P.; Rupp, S.; Hess, C. Operando Multiwavelength and Time-Resolved Raman Spectroscopy: Structural Dynamics of a Supported Vanadia Catalyst at Work. *J. Phys. Chem. C* **2018**, *122*, 3386−3400.

DOI: 10.1021/acscatal.9b00326
ACS Catal. 2019, 9, 4875−4886

(56) Weckhuysen, B. M.; Keller, D. E. Chemistry, spectroscopy and the role of supported vanadium oxides in heterogeneous catalysis. *Catal. Today* **2003**, *78*, 25−46.
(57) Wu, Z.; Dai, S.; Overbury, S. H. Multiwavelength Raman Spectroscopic Study of Silica-Supported Vanadium Oxide Catalysts. *J. Phys. Chem. C* **2010**, *114*, 412−422.
(58) Maganas, D.; Trunschke, A.; Schlögl, R.; Neese, F. A unified view on heterogeneous and homogeneous catalysts through a combination of spectroscopy and quantum chemistry. *Faraday Discuss.* **2016**, *188*, 181−197.
(59) Jaegers, N. R.; Wan, C.; Hu, M. Y.; Vasiliu, M.; Dixon, D. A.; Walter, E.; Wachs, I. E.; Wang, Y.; Hu, J. Z. Investigation of Silica-Supported Vanadium Oxide Catalysts by High-Field 51V Magic-Angle Spinning NMR. *J. Phys. Chem. C* **2017**, *121*, 6246−6254.
(60) Dai, H.; Bell, A. T.; Iglesia, E. Effects of molybdena on the catalytic properties of vanadia domains supported on alumina for oxidative dehydrogenation of propane. *J. Catal.* **2004**, *221*, 491−499.
(61) Grüne, P.; Wolfram, T.; Pelzer, K.; Schlögl, R.; Trunschke, A. Role of dispersion of vanadia on SBA-15 in the oxidative dehydrogenation of propane. *Catal. Today* **2010**, *157*, 137−142.
(62) Jentoft, F. C. Chapter 3 Ultraviolet−Visible−Near Infrared Spectroscopy in Catalysis: Theory, Experiment, Analysis, and Application Under Reaction Conditions. In *Advances in Catalysis*; Academic Press, 2009; Vol. *52*, pp 129−211.
(63) Gao, X.; Wachs, I. E. Investigation of Surface Structures of Supported Vanadium Oxide Catalysts by UV-vis-NIR Diffuse Reflectance Spectroscopy. *J. Phys. Chem. B* **2000**, *104*, 1261−1268.
(64) Gao, X.; Bare, S. R.; Weckhuysen, B. M.; Wachs, I. E. In Situ Spectroscopic Investigation of Molecular Structures of Highly Dispersed Vanadium Oxide on Silica under Various Conditions. *J. Phys. Chem. B* **1998**, *102*, 10842−10852.
(65) Haddad, N.; Bordes-Richard, E.; Hilaire, L.; Barama, A. Oxidative dehydrogenation of ethane to ethene on alumina-supported molybdenum-based catalysts modified by vanadium and phosphorus. *Catal. Today* **2007**, *126*, 256−263.
(66) Kondratenko, E. V.; Cherian, M.; Baerns, M. Oxidative dehydrogenation of propane over differently structured vanadia-based catalysts in the presence of O2 and N2O. *Catal. Today* **2006**, *112*, 60−63.
(67) Liu, J.; Mohamed, F.; Sauer, J. Selective oxidation of propene by vanadium oxide monomers supported on silica. *J. Catal.* **2014**, *317*, 75−82.
(68) Kube, P.; Frank, B.; Wrabetz, S.; Kröhnert, J.; Hävecker, M.; Velasco-Vélez, J.; Noack, J.; Schlögl, R.; Trunschke, A. Functional Analysis of Catalysts for Lower Alkane Oxidation. *ChemCatChem* **2017**, *9*, 573−585.
(69) Grant, J. T.; Carrero, C. A.; Love, A. M.; Verel, R.; Hermans, I. Enhanced Two-Dimensional Dispersion of Group V Metal Oxides on Silica. *ACS Catal.* **2015**, *5*, 5787−5793.
(70) Khodakov, A.; Yang, J.; Su, S.; Iglesia, E.; Bell, A. T. Structure and properties of vanadium oxide-zirconia catalysts for propane oxidative dehydrogenation. *J. Catal.* **1998**, *177*, 343−351.
(71) Alvarez-Amparán, M. A.; Cedeño-Caero, L.; Cortes-Jácome, M. A.; Toledo-Antonio, J. A. Relationship between the catalytic activity and Mo−V surface species in bimetallic catalysts for the oxidative desulfurization of dibenzothiophenic compounds. *React. Kinet., Mech. Catal.* **2017**, *122*, 869−885.
(72) Bensalem, A.; Weckhuysen, B. M.; Schoonheydt, R. A. In Situ Diffuse Reflectance Spectroscopy of Supported Chromium Oxide Catalysts: Kinetics of the Reduction Process with Carbon Monoxide. *J. Phys. Chem. B* **1997**, *101*, 2824−2829.
(73) Argyle, M. D.; Chen, K.; Resini, C.; Krebs, C.; Bell, A. T.; Iglesia, E. Extent of Reduction of Vanadium Oxides during Catalytic Oxidation of Alkanes Measured by in-Situ UV-Visible Spectroscopy. *J. Phys. Chem. B* **2004**, *108*, 2345−2353.
(74) Stoll, S.; Schweiger, A. EasySpin, a comprehensive software package for spectral simulation and analysis in EPR. *J. Magn. Reson.* **2006**, *178*, 42−55.
(75) Dinse, A.; Wolfram, T.; Carrero, C.; Schlögl, R.; Schomäcker, R.; Dinse, K. P. Exploring the Structure of Paramagnetic Centers in SBA-15 Supported Vanadia Catalysts with Pulsed One- and Two-Dimensional Electron Paramagnetic Resonance (EPR) and Electron Nuclear Double Resonance (ENDOR). *J. Phys. Chem. C* **2013**, *117*, 16921−16932.
(76) Lee, J. K.; Russo, V.; Melsheimer, J.; Köhler, K.; Schlögl, R. Genesis of V4+ in heteropoly compounds CsH4−PVMo11O40 during thermal treatment, rehydration and oxidation of methanol studied by EPR spectroscopy. *Phys. Chem. Chem. Phys.* **2000**, *2*, 2977−2983.
(77) Grasselli, R. K. Site isolation and phase cooperation: Two important concepts in selective oxidation catalysis: A retrospective. *Catal. Today* **2014**, *238*, 10−27.

DOI: 10.1021/acscatal.9b00326
ACS Catal. 2019, 9, 4875−4886